

GT2011-4) - -)

Experimental and Numerical Crossover Jet Impingement in a Rib-Roughened Airfoil Trailing-Edge Cooling Channel

M.E. Taslim and M.K.H. Fong

Mechanical and Industrial Engineering Department
Northeastern University
Boston, MA, USA

Abstract

Local and average heat transfer coefficients were measured in a test section simulating a rib-roughened trailing edge cooling cavity of a turbine airfoil. The test rig was made up of two adjacent channels, each with a trapezoidal cross sectional area. The first channel, simulating the cooling cavity adjacent to the trailing-edge cavity, supplied the cooling air to the trailing-edge channel through a row of racetrack-shaped slots on the partition wall between the two channels. Eleven crossover jets, issued from these slots entered the trailing-edge channel, impinged on eleven radial ribs and exited from a second row of race-track shaped slots on the opposite wall in staggered or inline arrangement. Two jet angles of 0 and 5° and a range of jet Reynolds number from 10,000 to 35,000 were tested and compared. The numerical models contained the entire trailing-edge and supply channels with all slots and ribs to simulate exactly the tested geometries. They were meshed with all-hexa structured mesh of high near-wall concentration. A pressure-correction based, multi-block, multi-grid, unstructured/adaptive commercial software was used in this investigation. Standard high Reynolds number $k - \epsilon$ turbulence model in conjunction with the generalized wall function for most parts was used for turbulence closure. Boundary conditions identical to those of the experiments were applied and several turbulence model results were compared. The numerical analyses also provided the share of each crossover and each exit hole from the total flow for different geometries. The major con-

clusions of this study were: a) except for the first and last cross-flow jets which had different flow structures, other jets produced the same heat transfer results on their target surfaces, b) tilted crossover jets produced higher heat transfer coefficients on the target surface towards which they were tilted and lower values on the opposite surface and c) the numerical predictions of impingement heat transfer coefficients were in good agreement with the measured values for most cases thus CFD could be considered a viable tool in airfoil cooling circuit designs.

Nomenclature

A_{heater} surface foil heater's area
 AR trailing-edge channel aspect ratio, $(b_{min} + b_{max})/2H = 0.245$
 b_{max} test section maximum base, 1.981 cm
 b_{min} test section minimum base, 1.143 cm
 D_h trailing-edge channel hydraulic diameter, 2.5 cm
 d_{cross} hydraulic diameter of each crossover hole, 1.315 cm
 e rib height, 0.584 cm
 h heat transfer coefficient, $W/(m^2 \cdot C)$
 H test section height, 6.35 cm (Figure 1)
 i current through the surface foil heater, amps
 k air thermal conductivity, $W/(m \cdot C)$
 m_i air mass flow rate through the i^{th} crossover hole, Kg/s
 \bar{Nu} local average Nusselt number based on the crossover hole hydraulic diameter, hd_{cross}/k
 P_{amb} ambient pressure, Pa

P_{supply} pressure in the supply channel upstream of the 6th crossover hole, Pa
 P_{TE} pressure in the trailing-edge channel downstream of the 6th crossover hole, Pa
 P_{cross} perimeter of each crossover hole, 2.859 cm
 q'' total heat flux generated by the foil heater ($= vi/A_{heater}$)
 q''_b total heat loss through the back of the target plate to the ambient
 q''_r total radiational losses from the heated target wall to the surrounding unheated walls
 r slots corner radii, 0.521 cm (Fig. 1)
 r_{rib} rib top corner radii, 0.19 cm (Fig. 1)
 Re_{jet} local jet Reynolds number based on the crossover hole hydraulic diameter and mass flow rate through the same crossover hole, $4m_i/P_{cross}\mu$)
 T/C thermocouple (Fig. 1)
 v voltage across the surface foil heater, volts
 V velocity magnitude
 w rib width, 0.584 cm
 β jet tilt angle (Fig. 1)

1 Introduction

Various methods have been developed over the years to keep turbine airfoil temperatures below critical levels. The main objective in turbine airfoil internal cooling is usually to achieve maximum heat transfer coefficients while minimizing the coolant flow rate. One such method is to route coolant air through a smooth or rib-roughened serpentine passages within the airfoil and convectively remove heat from the blade. The coolant is then ejected either at the tip of the blade, through the cooling slots along the trailing edge or cooling holes along the airfoil surface. Impingement cooling is another effective method of airfoil cooling. In this method, the coolant enters the leading- or trailing-edge cooling cavities as jets from the adjacent cavity through a series of crossover holes on the partition wall between the two cavities. The crossover jets impinge on the cavity walls (smooth or rib-roughened) and exit through the film holes on the pressure and suction sides, through the exit holes along the trailing edge, or form a cross flow in the cavity and move toward the airfoil tip. Several studies on impingement cooling of airfoils in the leading-edge and mid-chord cavities are reported. Chupp et al. [1] reported on the evaluation of internal heat transfer coefficients for impingement cooled turbine blades. Metzger and Bunker [2,3] reported on local impingement heat transfer in internally cooled turbine airfoil leading edge regions with and without film cooling. Chang et al. [4] investigated the effects of an array of circular jets impinging on a rib-roughened surface normally with the presence of a cross-flow. This arrangement was intended to simulate the jet impingements in the blade mid-chord cavities where a cross flow is also present. They concluded that the heat transfer effects of jet impingement on rib-roughened surfaces can be considerably improved by proper positioning on the jets with respect to the ribs. Akella and Han [5] reported on impingement cooling in rotating two-pass rectangular channels

with ribbed walls. Taslim et al. [6-11] reported the results of a series of investigations on internal impingement on the leading-edge cavity walls.

As dictated by the external shape of airfoil trailing-edge, trailing-edge cooling cavities often have very narrow trapezoidal shapes with characteristically small passage aspect ratios. The narrow trapezoidal shape of the trailing-edge cooling cavities puts restrictions on the use of ribs. Most of the reported work on the trailing cooling cavities, deal with the cooling flow across a pin bank and the ejection of cooling flow through the trailing-edge holes. Metzger et al. [12] reported on heat transfer and flow friction characteristics of very rough transverse ribbed surfaces with and without pin fins. Abuaf et al. [13] reported the results of an experimental investigation of the pressure drop and heat transfer coefficient distributions in serpentine passages with and without turbulence promoters. They investigated a three-legged passage with slanted bleed holes along the third leg. Air entered the test section at three inlet ports along the first leg and liquid crystals along with thin foil heaters were used to measure the heat transfer coefficient. Tests were run with and without wooden ribs mounted on the liquid crystals at an angle 90° with the flow direction. Lau et al. [14,15] reported on turbulent heat transfer and friction in pin fin channels with lateral flow ejection. Kumaran et al. [16] reported on augmented heat transfer in a pin fin channel with short or long ejection holes. Taslim et al. [17] studied the effects of bleed holes on the heat transfer coefficient and friction factor in a rib-roughened trapezoidal passage simulating the trailing edge cooling cavity of a turbine blade. The ribs were tapered and the cooling flow in the channel was radial. They concluded that there existed a large spanwise variation in heat transfer coefficient in the trailing edge cavity without the bleed holes. A more uniform distribution of the spanwise heat transfer coefficient was observed in test sections with the bleed holes. Another major conclusion was that the Nusselt number along the channel with bleed holes correlated well with the local Reynolds number. None of these cases, however, resembles the geometries or the flow pattern tested in the present work. Impingement on the trailing-edge walls with crossover jets have not been investigated to the same extent. Taslim and Nicolas [18] reported on an experimental and numerical investigation of jet impingement on ribs in an airfoil trailing-edge cooling channel. In this arrangement, the cooling air enters the trailing-edge cooling cavity from the adjacent cavity through a set of crossover holes and is then ejected through a series of holes along the airfoil trailing-edge and/or a few holes at the airfoil tip. This complex geometry creates a complex flow field. Both longitudinal and spanwise variations in air velocity and heat transfer coefficient are expected. Taslim and Nongsang [19] reported on a combined experimental and numerical study on crossover jet impingement heat transfer in a narrow trapezoidal channel simulating a typical trailing-edge cooling cavity with smooth walls. Zero and five-degree jet angles were tested. Major conclusions in that study was that jets tilted at an angle of 5 degrees produced higher heat transfer coefficients on the target surface. The tilted jets also produced the same level of

fraction of a degree. A typical jet temperature was 21°C.

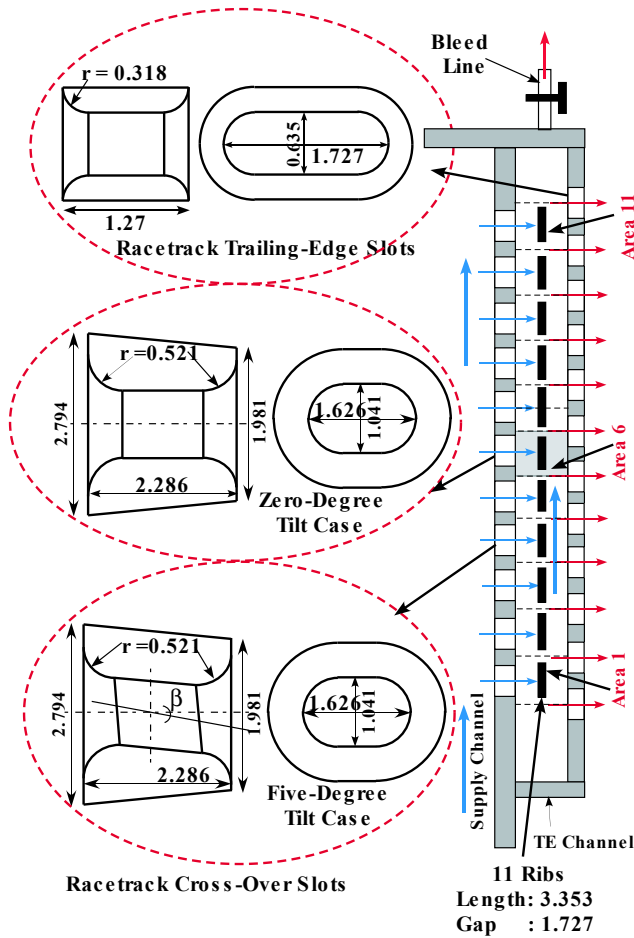


Fig. 2. Details of the test section.

5-cm-thick styrofoam slab to minimize heat losses to the environment. The radiational heat loss from the heated wall to the unheated walls as well as losses to ambient air were taken into consideration when heat transfer coefficients were calculated. A digital camera, in conjunction with proper filters and background lighting to simulate daylight conditions, was used to take pictures of isochrome patterns formed on the liquid crystal sheet. A centrifugal compressor supplied compressed air to a 0.76m³ storage tank. A combination of an air dryer and two air filters dried and cleaned the air. A pressure regulator was used to set the air mass flow rate for a desired jet Reynolds number. A critical venturi, choked for all mass flow rates, was then used to measure the air mass flow rate before it entered the test section plenum at about ambient temperature. Total mass flow rate entering the supply channel varied from 0.023 to 0.08Kg/s. Heat was induced to the air in the test section via the heaters through a custom-designed power supply unit. Each heater was individually controlled by a variable transformer to assure a constant heat flux over the entire heated wall. Four thermocouples along the supply channel including one immediately upstream of the sixth crossover hole measured the jet temperature. Their measurements did not differ by more than a

3 Computational Model

The computational model was constructed for the entire setup. The model included the supply channel, the crossover holes, the rib-roughened trailing-edge channel and the exit holes. Figure ?? shows a typical mesh for the staggered flow arrangement with all eleven crossover and twelve trailing-edge slots while Fig. 4 shows the details of the mesh distribution around a computational cell made up of a crossover hole, a trailing-edge slot and their share of the supply and trailing-edge channels. The CFD analyses was performed using Fluent/UNS solver by Ansys, Inc., a pressure-correction based, multi-block, multi-grid, unstructured/adaptive solver. Boundary conditions for the numerical models were identical to those of the experiments. At the inlet, a total mass flow rate exactly the same as what was measured (0.034 – 0.08 kg/s range) was specified at the same temperature (18 – 25 °C range) and pressure (101.35 – 105.4 KPa range) of the air entering the rig. The heat fluxes on the heated walls were also identical to those of experiment (2500 – 4000 W/m² range). Exit holes had a pressure boundary condition identical to that of the lab. Standard high Reynolds number $k - \epsilon$ turbulence model in conjunction with the generalized wall function was used for turbulence closure. The average y^+ for the first layer of cells was calculated to be below 5 for all cases since the enhanced wall treatment method was employed. Other available turbulence models in this commercial code including the $k - \omega$ with Shear Stress Transport (SST) option and $v2f$ models were also tested and the corresponding results are compared. Mesh independence was achieved at about 12 million cells for a typical model. Cells in all models were entirely hexagonal, a preferred choice for CFD analyses, and were varied in size bi-geometrically from the boundaries to the center of the computational domain in order to have finer mesh close to the boundaries. Residual sums for all variables in all models were less than 1×10^{-7} . Convergence, for most cases, was achieved at around 15000 iterations.

4 Results and Discussion

In this paper, experimental and numerical results are presented for two flow arrangements. The flow arrangements are shown in Fig. 5. In the inline case, flow entered the trailing-edge channel from the eleven crossover holes, diffused into the trailing-edge channel to interact with both the the rib-roughened and smooth target walls, and was ejected from the trailing-edge channel through eleven exit slots that were geometrically arranged inline with the crossover holes. In the staggered case, flow entered the trailing-edge channel from the same eleven crossover holes. However, it was ejected from the trailing-edge channel through twelve exit slots that were geometrically staggered with respect to the crossover holes. Each of these cases were run for zero- and five-degree tilt angles. These were considered as our baseline

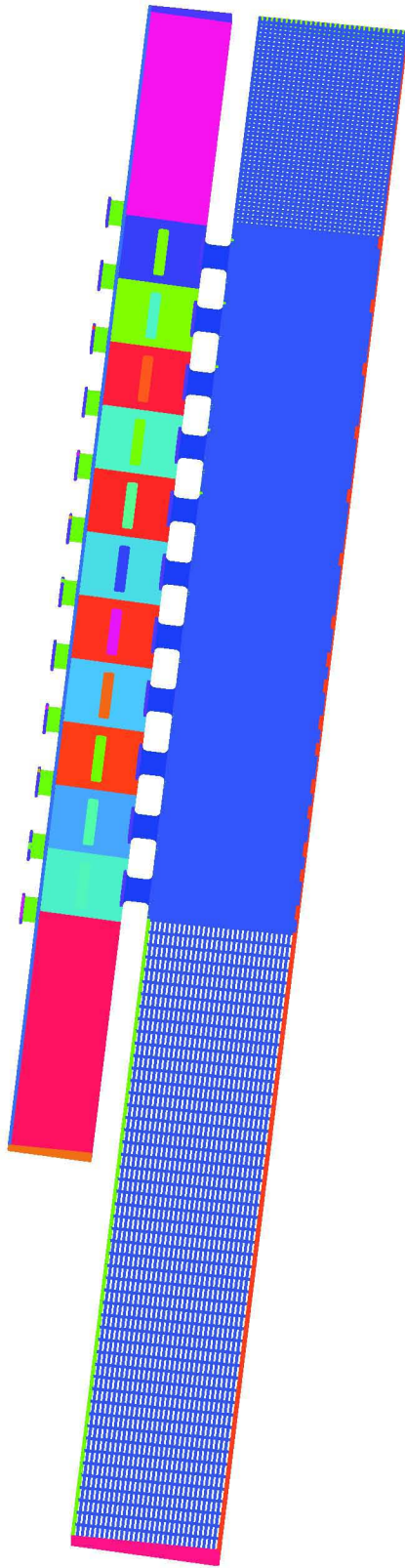


Fig. 3. A typical mesh for the entire test section with the crossover and exit holes.

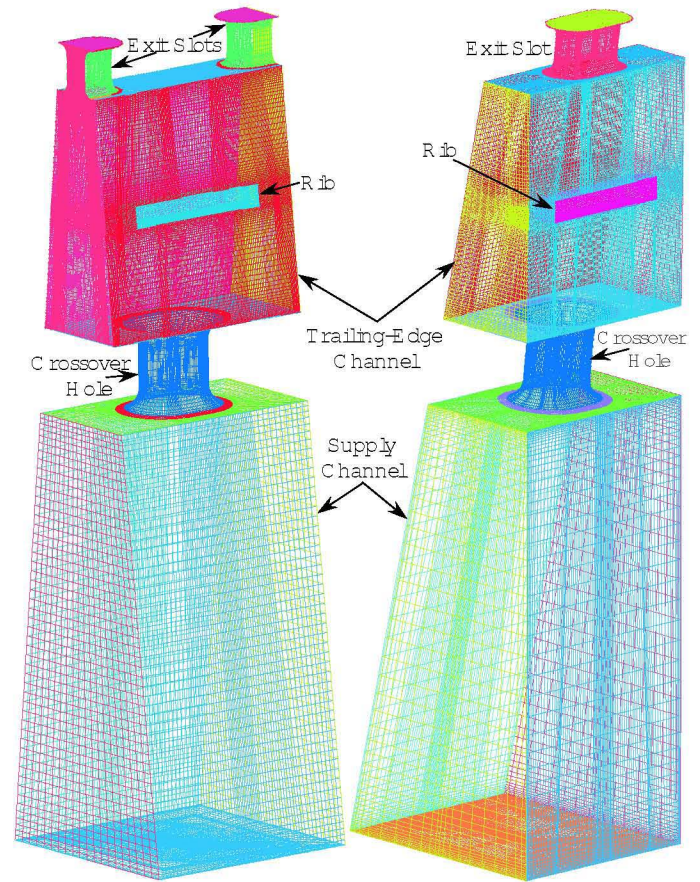


Fig. 4. Details of the mesh around a crossover and a trailing-edge slot for inline and staggered flow arrangements.

cases. For these baseline cases, all measurements were done on area 6 (see Fig. 2) since the heat transfer coefficient did not show a measurable change from area 2 through area 10 when it was correlated with the local jet Reynolds number. Actual photos of liquid crystals displays confirmed a remarkable similarity of iso-chromes on these areas and numerical results confirmed this behavior as we will show shortly.

In real life practice, there may be occasions that the trailing edge exit holes do not line up with the crossover holes or some of them might be plugged for a variety of reasons including casting imperfections or presence of foreign objects. To investigate the effects of the exit hole blockage on local heat transfer performance, tests were performed for cases in which the first 2 or 4 exit slots (slots 1 through 4 in Fig. 1) were blocked while all crossover holes remained open. At the same time, the bleed line simulating the airfoil tip hole was open and tip flow was adjusted. Changes in flow structure due to the blockage of a portion of the exit slots was quite evident and caused a significant variation in heat transfer coefficient on areas 1 through 5. These flow arrangements created a different flow structure that affected the heat transfer coefficients on the target walls downstream of the crossover jets.

As was mentioned earlier, for all cases in which all trailing-edge slots were open, measurements were performed in the middle of the test section on area 6 in Fig. 2. This lo-

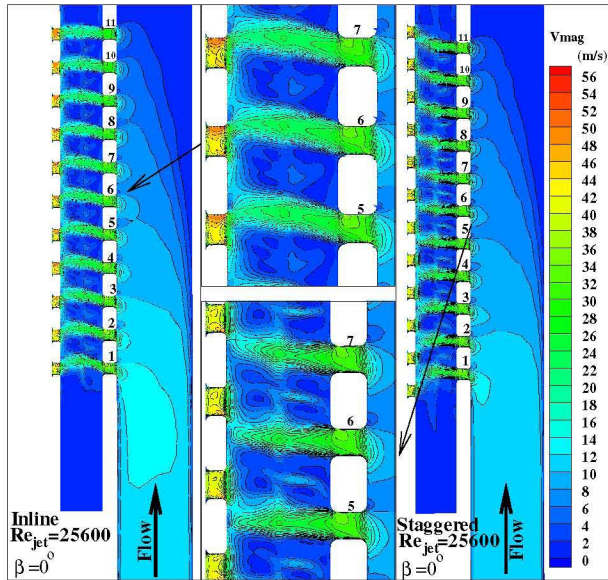


Fig. 5. Typical CFD contours of velocity magnitude on the rig mid-plane for inline arrangement with 0° tilt angle and for staggered arrangement with 5° tilt angle.

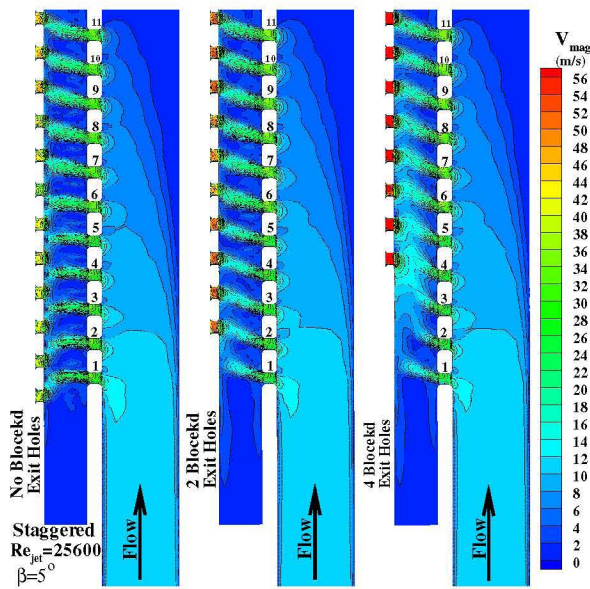


Fig. 6. Typical CFD contours of velocity magnitude on the rig mid-plane for 0, 2 and 4 blocked exit holes, staggered flow arrangement and 5° tilt angle.

cation aligned axially with the center of crossover hole number 6. Thus the jet Reynolds number is based on the mass flow rate through the crossover hole number 6. Depending on the number of open exit holes, the share of the crossover holes from the total mass flow varies from 6.85 to 11.26 percent. To determine these percentages, thorough analyses of the flow fields for different flow arrangements had to be done. A three-dimensional CFD model of each flow arrangement was run under the tests boundary conditions. Figures 5 and 6 show the contours of velocity magnitude on the channel mid-plane for four representative cases. These contour plots

are on a plane that passes through the centers of crossover holes and trailing-edge slots. Changes in flow structure and formation of an axial flow in the trailing-edge channel where the trailing-edge slots are blocked is evident. Crossover jets on the opposite side of the blocked exit holes are diverted towards the open trailing-edge slots and are not effectively impinging on target surfaces as they are in the cases in which all exit holes are open. We will discuss the effects of the changes in flow structure, due to the blocked exit holes, on the mass flow rates through the crossover holes, and on the heat transfer coefficients on the target walls in the ensuing sections.

Figure 7 shows the percentage of total mass flow rate passing through the crossover holes for different geometries and flow arrangements. These figures were generated from the CFD results. For a given geometry and flow arrangement, these percentages did not show any significant variation with the jet Reynolds number. Therefore, each set of symbols represents the average values for all tested jet Reynolds numbers. The horizontal dashed line in the figure, serving as a reference, corresponds to the value of 9.09% if the total flow passed in equal amounts through the eleven crossover holes. It can be seen that, the mass flow rate through the middle crossover hole is very close to the average value. When all exit holes were open, this percentage varied slightly for the crossover holes on both sides of the middle hole. The first crossover hole in the staggered arrangement received the maximum percentage of 9.6%. This is explained by the velocity contours of Fig. 5 in which the jet issued from the first crossover hole in the staggered arrangement finds its way out through two exit holes compared to one exit hole in the inline arrangement. In other words, the flow through the first crossover hole experiences less resistance on its way out of the trailing-edge channel. When 2 or 4 exit holes are blocked, while the middle crossover hole's share of the total flow is again very close to the average value of 9.09%, a more severe variation in flow percentages is observed. Crossover holes 1 through 5 receive less than the average flow percentage while the crossover holes 7 through 11 receive more than the average flow percentage. This monotonic increase of flow through the crossover holes in axial direction was observed for all tested flow rates. As Fig. 6 shows, the blocked exit holes against the crossover holes 1 through 4 create a resistance to the jet issued out of these holes and reduce the mass flow rate for those crossover holes. The crossover jets are tilted axially in the flow direction and, as a result, produce lower heat transfer coefficients on their target surfaces to be discussed shortly. The jet Reynolds number for which the surface Nusselt numbers for the target areas 1 through 11 are presented, are all based on the air mass flow rate through their corresponding crossover hole. Of particular interest is the case with 4 blocked exit holes in which the mass flow rate through the first crossover hole is about 33% less than that through the last crossover hole. The axial (upward) velocity component in the trailing-edge channel causes the curvature on the velocity contours and pushes the flow towards the downstream exit holes.

Fig. 8 shows the flow distribution through the exit holes

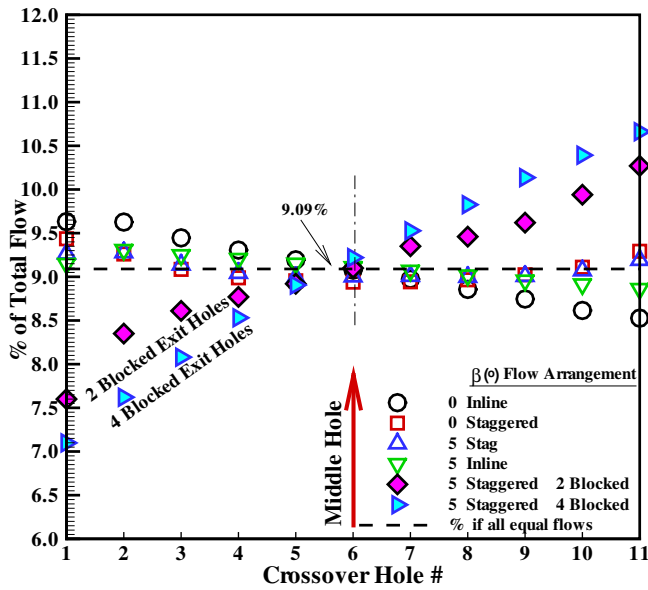


Fig. 7. Percentage of mass flow rate through the crossover holes with all exit holes open.

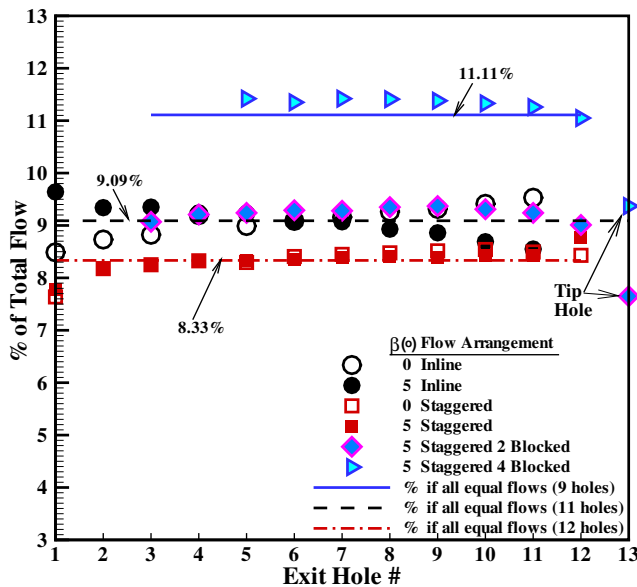


Fig. 8. Percentage of mass flow rates through the exit holes.

for all geometries and flow arrangements. The horizontal lines represent the percentage of the flow through each hole if they received an equal share of the flow in each arrangement. These values change depending on the number of open exit holes. In general, the exit hole mass variation is not as drastic as the crossover holes mass distribution. Only those on both ends show a small change. It should be noted that

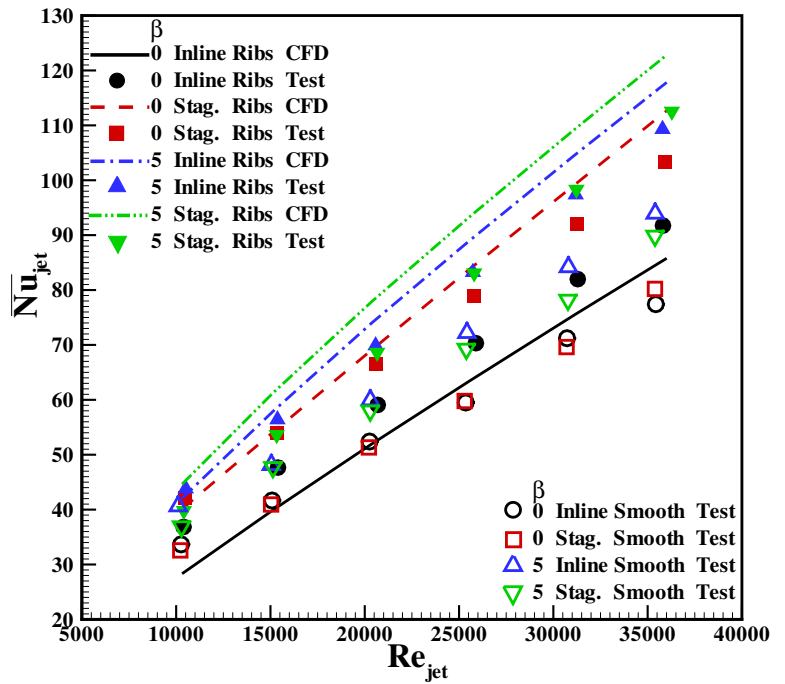


Fig. 9. Measured versus CFD Nusselt number variation with local jet number on area 6, no blocked exit hole.

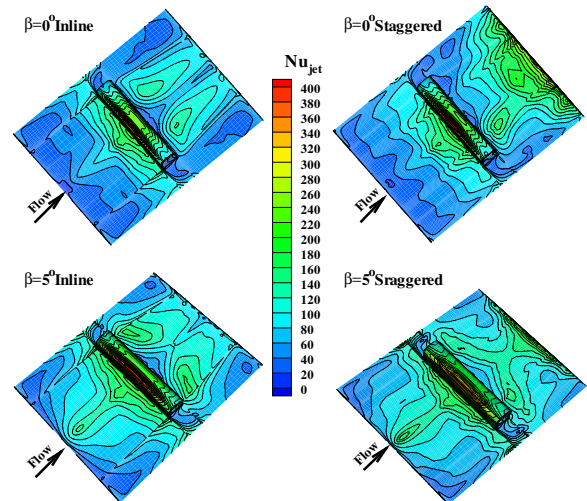


Fig. 10. Typical CFD contours of Nusselt numbers on the floor and rib surfaces of area 6 for 0° and 5° tilt angles, and for inline and staggered flow arrangements.

hole number 13 represents the trailing-edge channel end hole simulating the airfoil tip hole. If the percentage of the flow through the tip hole is less than the exit holes, it is because it was set to have a nominal mass flow percentage of about 8% of the total flow. This hole was open only when 2 or 4 exit holes were blocked.

The heat transfer coefficient corresponding to each recorded picture of liquid crystals display was calculated from:

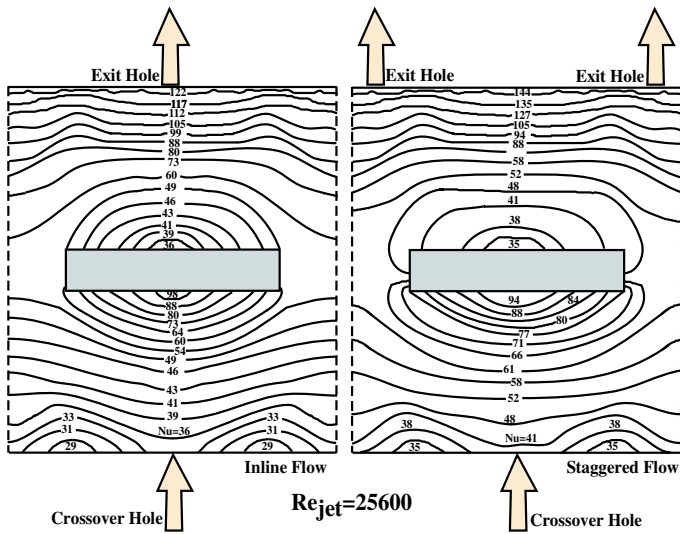


Fig. 11. Measured contours of Nusselt numbers on area 6 for 0° tilt angle, and for inline and staggered flow arrangements.

$$h = \frac{q'' - q_b'' - q_r''}{(T_s - T_j)}$$

where T_s and T_j are the surface and jet temperatures, respectively. q'' is the total heat flux generated by the foil heater, q_b'' is the total heat loss through the back of the target plate to the ambient and q_r'' is the total radiational losses from the heated target wall to the surrounding unheated walls. Air properties including the viscosity and thermal conductivity for the calculation of the Reynolds and Nusselt numbers were evaluated at the jet temperature. Experimental uncertainties in Reynolds numbers and heat transfer coefficients, following the method of Kline and McClintock [20], were calculated to be about $\pm 3\%$ and $\pm 6\%$, respectively.

The experimental heat transfer results for the baseline (all open exit holes) cases are presented in Fig. 9. Measurements were performed on area 6 in the middle of the test section for two jet tilt angles of zero and 5 degrees and for two crossover versus trailing-edge slot arrangements of inline and staggered. For comparison, on the same figure, we have included the test results of our previous study (Taslim and Nongsaeng, 2010) in the same test section with no ribs (hollow symbols). The presence of the ribs on the target wall has caused increases in heat transfer coefficients up to 30%. This increase is due to the interaction of the jet with the rib and formation of vortices around and downstream of the rib. Liquid crystal display of surface temperature showed identical patterns for areas 2 through 10 thus the camera was focused on area 6 for a detailed analysis of the heat transfer pattern and the reported heat transfer results represent the Nusselt number downstream of the crossover jets 2 through 10. It should be mentioned that, in this and ensuing figures, the symbols represent the measured data while the lines represent the numerically-obtained results. As expected, the tilted

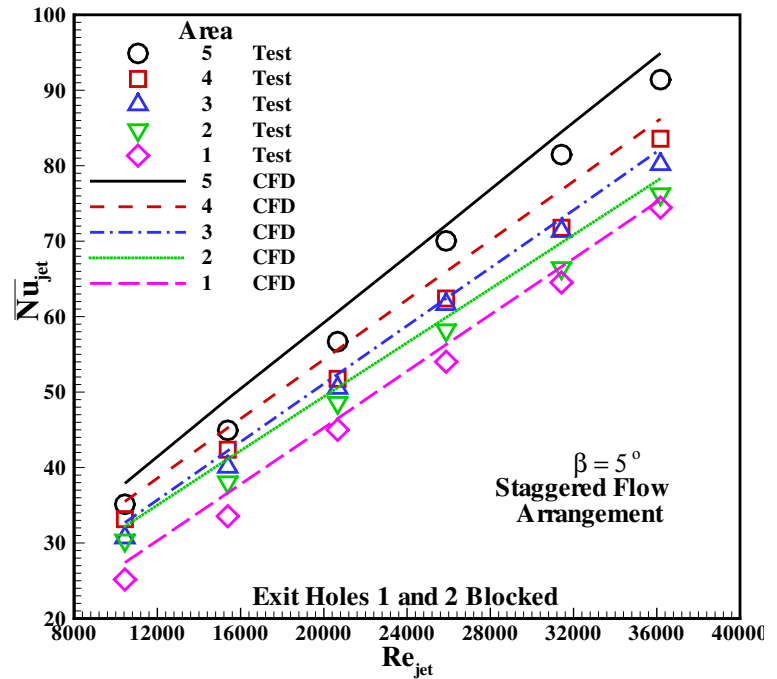


Fig. 12. Measured Nusselt number variation with local jet Reynolds number on areas 1 through 5 for the 5° tilt angle, 2 blocked exit holes and open end hole.

jets produce higher heat transfer coefficients due to more effective interactions between the them and the rib-roughened target wall. The tilted jets rebound and diffuse in all directions after impingement and interact with the neighboring target walls while the 0° jets diffuse into the trailing-edge channel in a symmetric fashion and have much less interaction with the neighboring target walls. As for the inline versus staggered arrangements, the 5° -tilt results were very close while the 0° -tilt results show a 12% increase for the staggered case. This behavior is explained by the strong interaction between the jet and the rib in the 5° -tilt case such that the jet disperses in all forward directions thus the alignment of the exit holes does not affect the heat transfer coefficient downstream the rib. The differences between these cases are also seen in Fig. 10 where the CFD contours of Nusselt number on area 6 for typical inline and staggered arrangements are compared. The numerical results show the same trend with almost no difference for the 5° -tilt and inline case at the lowest end of the jet Reynolds number range and a maximum difference of about 23% for the 0° -tilt case, again at the lowest end of the jet Reynolds number range. Contours of measured Nusselt numbers on the target area 6 for the inline and staggered flow arrangements are shown in Fig. 11. What is reported as the average Nusselt number on area 6 is the area-weighted average of these contours lines on that area. High heat transfer coefficients immediately upstream of the rib and exit hole(s) are in agreement with the CFD contours of Fig. 10.

Measured heat transfer results for 2 and 4 blocked trailing-edge slots are shown in Figs. 12 and 13. Evidenced

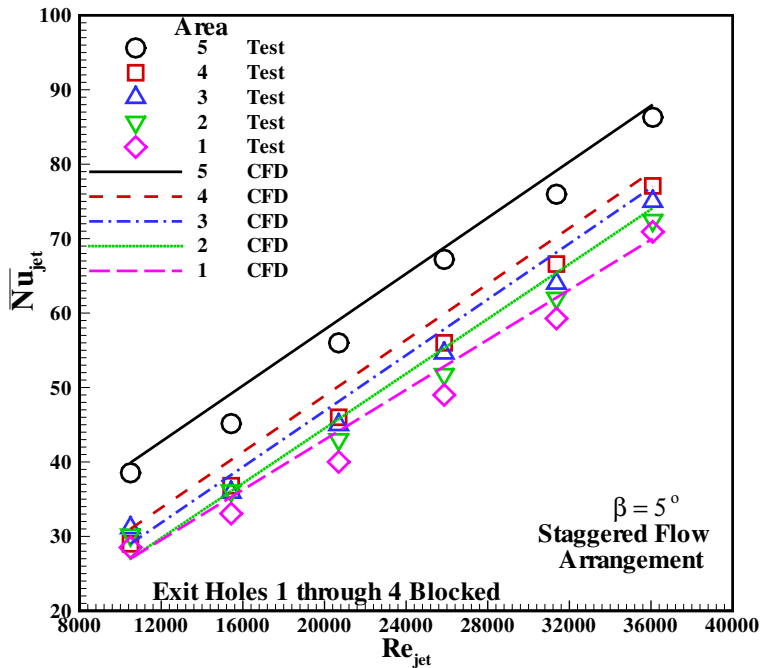


Fig. 13. Measured Nusselt number variation with local jet Reynolds number on areas 1 through 5 for the 5° tilt angle, 4 blocked exit holes and open end hole.

by the numerical results shown in Fig. 6, when these exit slots were blocked and the bleed line at the other end of the channel was open, the crossover jets issued from the first two or four crossover slots were forced to turn towards the open exit slots. In both cases, the heat transfer coefficients on the target areas corresponding to the blocked exit holes show a remarkable reduction. Those crossover jets opposite the blocked exit holes form an axial flow that diverts the downstream jets until the flow reaches the first open exit hole. This axial flow reduces the crossover jet interaction with the target area thus reducing the heat transfer coefficients on areas 1 and 2 in Fig. 12 and on areas 1 through 4 in Fig. 13. When two exit holes are blocked, area 1 which gets no benefit from either impingement or cross-flow, exhibits a very low heat transfer coefficient. The combined effects of impingement and cross-flow, however, increases the heat transfer coefficient on areas 2 through 5. When 4 trailing-edge slots are blocked, the same pattern, although more severe, is observed. Beyond the fifth area, the impingement effects took over and the remaining areas had the same level of heat transfer coefficients. Other geometries and flow arrangements exhibited the same behavior and are not presented here due to space limitation. Again, with the same trend and behavior, the numerical heat transfer results were higher than the test result for most cases with an overall difference of 9.5%

Figures 14, 15, 16 and 17 show the numerical heat transfer results along the channel for the baseline cases of zero and 5-degree tilt angles, inline and staggered flow arrangements. For the inline flow arrangements of both tilt angles, Areas 1 and 11, corresponding to the first and last crossover holes produced lower heat transfer coefficients than others

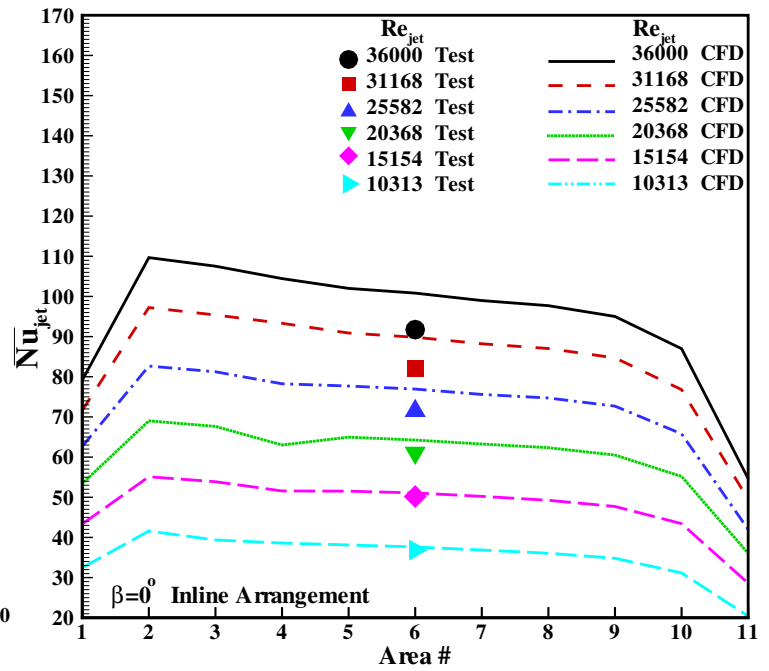


Fig. 14. Comparison of the CFD and test results for the 0° tilt angle and inline flow arrangement.

since only a portion of these areas were affected by the first and last crossover jets and they did not benefit from the crossover jets as much as the other areas did. Furthermore, evidenced by Fig. 7, crossover hole 11 receives the least amount of flow and that is another reason for the reduction of the heat transfer coefficient on that area. Liquid crystal displays confirmed the same behavior. The first crossover jet, although received more than average share of the mass flow rate, did not have an effective interaction with the first target area, instead, combined with the second crossover jet, consistently produced a higher heat transfer coefficient on area 2 in these four baseline cases. Higher than average mass flow rate through the second crossover hole also contributed to the high heat transfer coefficient on area 2. Heat transfer coefficients on the other areas (3 through 10) are close to each other within $\pm 10\%$. Test results for area 6 in the middle of the test section show a reasonable agreement with the numerical values in most cases with a maximum difference of about 15% in the staggered case of zero tilt angle. Identical scales of the axes in these figures helps comparing the inline versus staggered flow arrangements as well at the 0° versus 5° tilt-angle results.

Measurements and numerical analyses were also conducted on the wall opposite the target wall for the 5° tilt angle. Results are shown in Fig. 18. The heat transfer results on the opposite wall were not remarkably different from those on the target wall mainly due to the fact that the walls are very close to each other and the opposite wall benefits from jet rebound after it interacts with the rib. Contours of velocity magnitudes shown in Fig. 19 on the cutting planes that pass through the middle crossover and exit holes show the

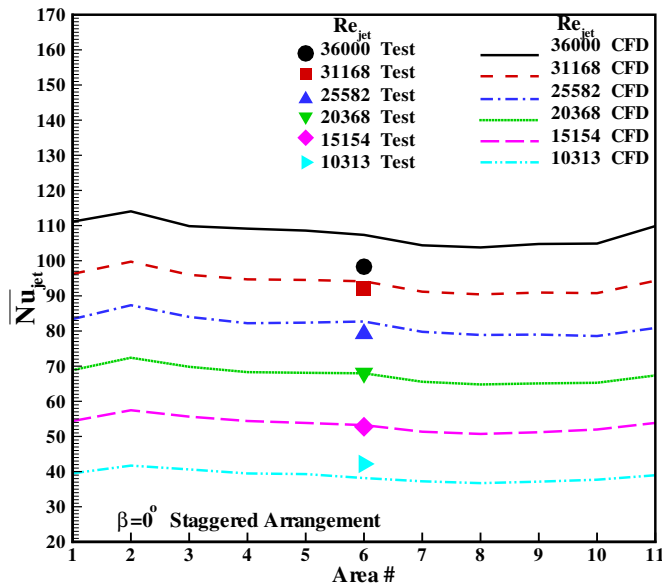


Fig. 15. Comparison of the CFD and test results for the 0° tilt angle and staggered flow arrangement.

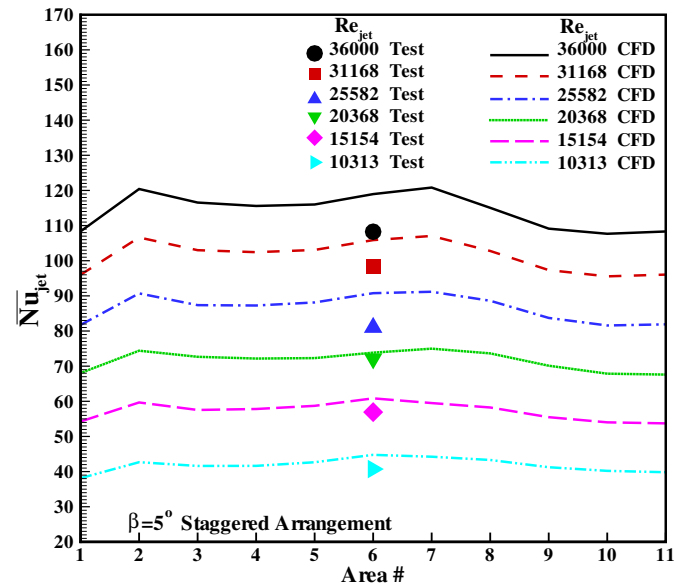


Fig. 17. Comparison of the CFD and test results for the 5° tilt angle and staggered flow arrangement.

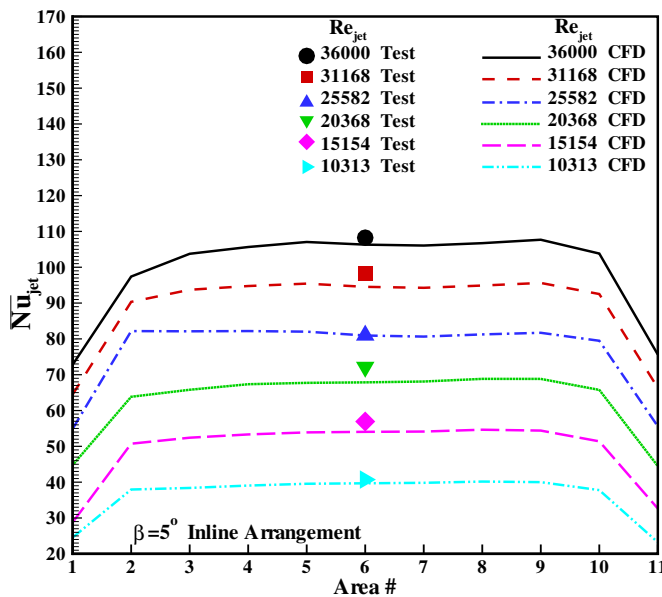


Fig. 16. Comparison of the CFD and test results for the 5° tilt angle and inline flow arrangement.

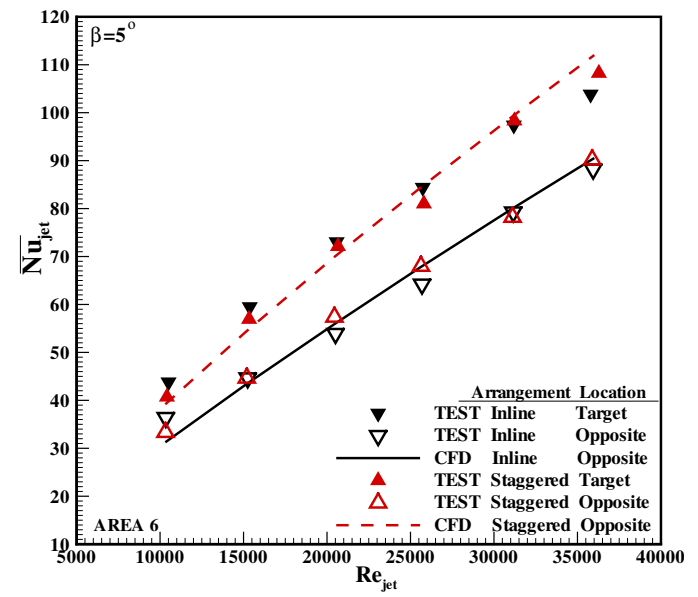


Fig. 18. Comparison of the CFD and test results on the target and opposite walls for the 5° tilt angle, inline and staggered flow arrangements.

crossover jet interaction with the two opposing walls. In the inline case, the crossover jet hugs the two walls as it diffuses into the channel towards the opposing exit holes. In the staggered arrangement for which the velocity contours are shown on two cutting planes, with the exit holes not located directly opposite the crossover holes, the jet is tilted towards the opposite wall as it interacts with the rib. However, on its way out through the staggered exit holes, it has an effective interaction with the target wall. These flow structures produced fairly high heat transfer coefficients, given that the opposite

was not rib-roughened. Similar to the heat transfer results on the target wall, a reasonable agreement between the test and numerical results on the opposite wall is also observed.

As was mentioned earlier, several turbulence models including the $k - \epsilon$, $k - \omega$ and $v2f$ models were used for all numerical cases and results for different geometries were compared. It was then concluded that the realizable $k - \epsilon$ model with the standard wall function along with the second order

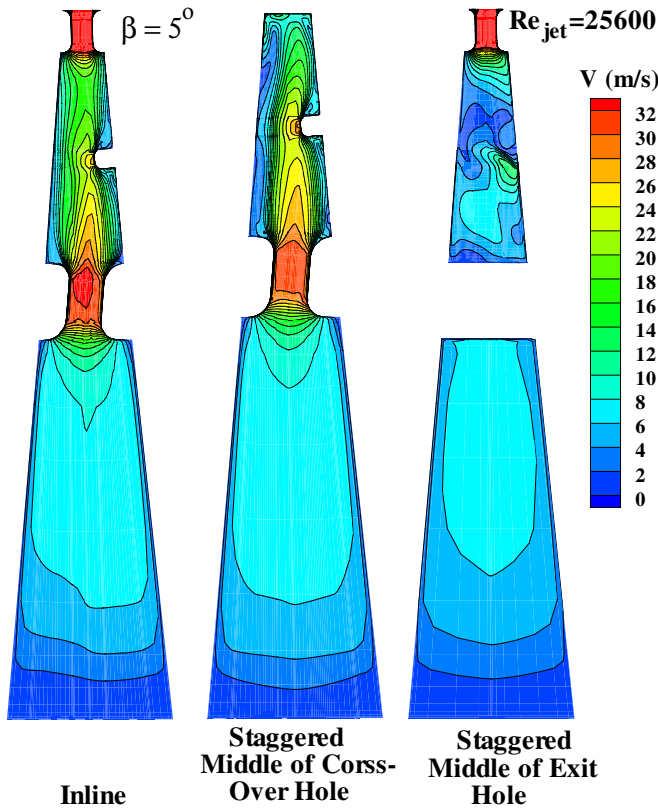


Fig. 19. Contours of velocity magnitude on the planes cutting the crossover and exit holes in the middle of the trailing-edge channel for the inline and staggered flow arrangements.

upwind discretization, produced, for most cases, the closest heat transfer results to the measured data. Figure 20 compares the numerical and tested results for one representative case of 5° tilt angle, staggered arrangement and four blocked exit holes. The superiority of the $k-\epsilon$ model for both areas 1 and 5 over the two other models is evident. Numerical results for other geometries and flow arrangements produced the same trend and are not presented here due to space limitation.

Finally, measured pressure ratios across the crossover holes (P_{supply}/P_{TE}) and pressure ratios across the trailing-edge channel (P_{supply}/P_{amb}) for all tested geometries and flow arrangements are shown in Fig. 21. The cluster of symbols on the lower side of the graph correspond to the pressure ratios across the crossover hole number 6 in the middle of the test section where pressure measurements were performed. These pressure ratios did not vary with the tilt angle (β), flow arrangement (inline or staggered) or the number of blocked exit holes. This is explained by the fact that the exit holes represent the limiting opening area along the flow path. Therefore, the most restriction to the flow is through the exit holes. Same reason explains the increase of pressure ratios across the whole trailing-edge channel as the number of blocked exit holes increases. There are three distinct clusters of symbols with the lower values corresponding to the case of all open exit holes and the highest values corresponding to the case of four blocked exit holes i.e. as the exit area

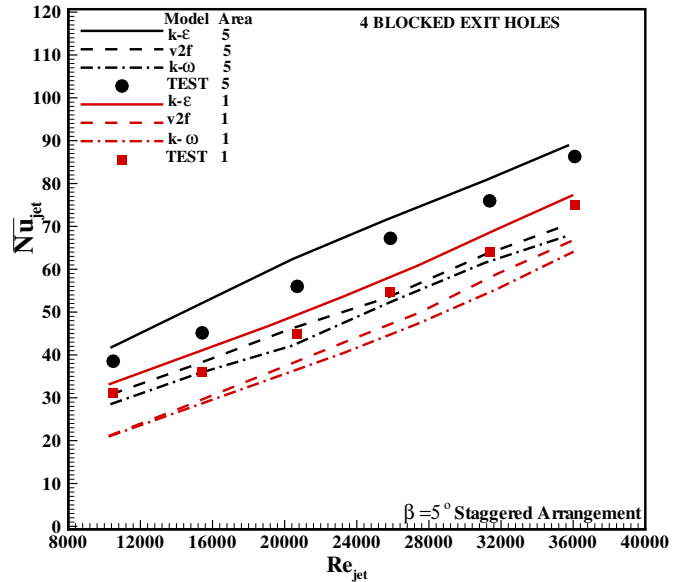


Fig. 20. Comparison of the $k-\epsilon$, $k-\omega$ and $v2f$ turbulence models with the test results for the 5° tilt angle, staggered arrangement and 4 blocked exit holes.

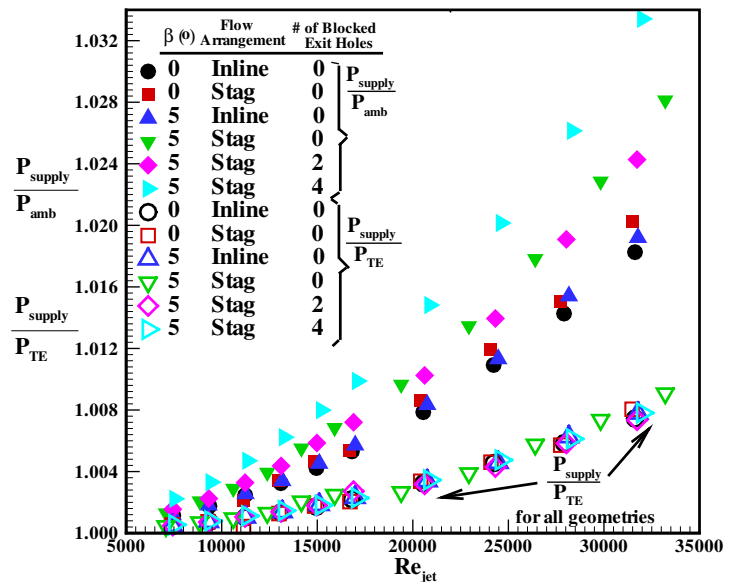


Fig. 21. Measured pressure ratios across the crossover holes and across the trailing-edge channel for all geometries and flow arrangements.

decreased, the pressures in the supply and trailing-edge channels increased at the same rate.

5 Conclusions

Effects of crossover jets for the cooling of a rib-roughened trailing-edge cavity were studied for two jet tilt

angles, inline and staggered crossover and exit holes, and cases of partially blocked exit holes. It was concluded that:

1) Presence of the ribs on the target wall downstream of the crossover holes has produced an increase of up to 30% in heat transfer coefficient.

2) Except for the first and last crossover jets in the inline arrangement which had different flow structures, other jets produced the same level of heat transfer results on their target surfaces,

3) Jets tilted at an angle of 5° produced higher heat transfer coefficients on the target surface. The tilted jets also produced a fairly high level of heat transfer coefficients on the smooth wall opposite the target wall.

4) Secondary cross-flow, caused by the blockage of trailing-edge slots, changed the flow structure and reduced the heat transfer coefficients on the target areas immediately upstream of the blocked exit holes.

5) Pressure ratios across the trailing-edge exit holes is much higher than those across the crossover holes since the exit holes represent the limiting opening area along the flow path.

6) Numerical heat transfer results with the use of standard high Reynolds number $k - \epsilon$ turbulence model in conjunction with the generalized wall function were generally in a reasonable agreement with the test results.

6 REFERENCES

[1] Chupp, R.E., Helms, H.E., McFadden, P.W., and Brown, T.R., 1969, "Evaluation of Internal Heat Transfer Coefficients for Impingement Cooled Turbine Blades," *J. Aircraft*, Vol. 6, No. 1, pp. 203-208.

[2] Metzger, D.E., and Bunker, R.S., 1990, "Local Heat Transfer in Internally Cooled Turbine Airfoil Leading Edge Regions: Part I - Impingement Cooling Without Film Coolant Extraction," *J. Turbomachinery*, Vol. 112, No. 3, pp. 451-458.

[3] Bunker, R.S., and Metzger, D.E., 1990, "Local Heat Transfer in Internally Cooled Turbine Airfoil Leading Edge Regions: Part II - Impingement Cooling With Film Coolant Extraction," *J. Turbomachinery*, Vol. 112, No. 3, pp. 459-466.

[4] Chang, H., Zhang, D., and Huang, T., 1997, "Impingement Heat Transfer From Rib Roughened Surface Within Arrays of Circular Jet: The Effect of the Relative Position of the Jet Hole to the Ribs," Paper # 97-GT-331.

[5] Akella, K.V. and Han, J.C., 1999, "Impingement Cooling in Rotating Two-pass Rectangular Channels with Ribbed Walls," *J. Thermophysics and Heat Transfer*, Vol. 13, No. 3, pp. 364-371.

[6] Taslim, M.E., L. Setayeshgar, and Spring, S.D., 2001, "An Experimental Evaluation of Advanced Leading-Edge Impingement Cooling Concepts," *J. Turbomachinery*, Vol. 123, pp. 147-153.

[7] Taslim, M.E., Pan, Y. and Spring, S.D., 2001, "An Experimental Study of Impingement on Roughened Airfoil Leading-Edge Walls with Film Holes," *J. Turbomachinery*, Vol. 123, No. 4, pp. 766-773.

[8] Taslim, M.E., Bakhtari, K., and H. Liu, 2003, "Experimental and Numerical Investigation of Impingement on a Rib-Roughened Leading-Edge Wall," *J. Turbomachinery*, Vol. 125, pp. 682-691.

[9] Taslim, M.E. and Khanicheh, A., 2006, "Experimental and Numerical Study of Impingement on an Airfoil Leading-Edge with and Without Showerhead and Gill Film Holes," *J. Turbomachinery*, Vol. 128, No. 2, pp. 310-320.

[10] Taslim, M.E. and Bethka, D., 2009, "Experimental and Numerical Impingement Heat Transfer in an Airfoil Leading-Edge Cooling Channel With Cross-flow," *J. Turbomachinery*, Vol. 131, No. 1, pp. 011021-1-011021-7.

[11] Taslim, M.E. and Abdelrassoul, A., 2009, "An Experimental and Numerical Investigation of Impingement Heat Transfer in Airfoils Leading-Edge Cooling Channel," *Int. Symp. on Heat Transfer in Gas Turbine Systems*, 9-14 August, 2009, Antalya, Turkey.

[12] Metzger, D.E., Fan, C.S. and Pennington, J.W., 1983, "Heat Transfer and Flow Friction Characteristics of Very Rough Transverse Ribbed Surfaces With and Without Pin Fins," *Proc. ASME/JSME Thermal Engineering Joint Conference*, Vol. 1, pp. 429-436.

[13] Abuaf, N., Gibbs, R. and Baum, R., 1986, "Pressure Drop and Heat Transfer Coefficient Distributions in Serpentine Passages With and Without Turbulence Promoters," *The Eighth International Heat Transfer Conference*, Edited by C.L. Tien, V.P. Carey and J.K. Ferrel, pp. 2837-2845.

[14] Lau, S.C., Han, J.C. and Kim, Y.S., 1989a, "Turbulent Heat Transfer and Friction in Pin Fin Channels with Lateral Flow Ejection," *J. Heat Transfer*, Vol. 111, No. 1, pp. 51-58.

[15] Lau, S.C., Han, J.C. and Batten, T., 1989b, "Heat Transfer, Pressure Drop and Mass Flow rate in Pin Fin Channels with Long and Short Trailing Edge Ejection Holes," *J. Turbomachinery*, Vol. 111, No. 2, pp. 117-123.

[16] Kumaran, T.K., Han, J.C. and Lau, S.C., 1991, "Augmented Heat Transfer in a Pin Fin Channel With Short or Long Ejection Holes," *Int. J. Heat Mass Transfer*, Vol. 34, No. 10, pp. 2617-2628.

[17] Taslim, M.E., Li, T. and Spring, D., 1995, "Experimental Study of the Effects of Bleed Holes on Heat Transfer and Pressure Drop in Trapezoidal Passages with Tapered Turbulators," *J. Turbomachinery*, Vol. 117, No. 2, pp. 281-289.

[18] Taslim, M.E. and Nicolas, G., 2008, "An Experimental and Numerical Investigation of Jet Impingement on Ribs in an Airfoil Trailing-Edge Cooling Channel," *The 12th. International Symposium on Transport Phenomena and Dynamics of Rotating Machinery*, Honolulu, Hawaii, Paper # ISROMAC12-2008-20238.

[19] Taslim, M.E. and Nongsaeng, A., 2010, "Experimental and Numerical crossover Jet Impingement in an Airfoil Trailing-Edge Cooling Channel," *ASME Turbo Expo 2010*, Glasgow, UK, June 14-18, 2010, Paper # GT2010-23521.

[20] Kline, S.J. and McClintock, F.A., 1953, "Describing Uncertainty in Single-Sample Experiments," *Mechanical Engineering*, Vol. 75, pp. 3-8.